

Identified Particle Distributions in pp and $Au + Au$ Collisions at $\sqrt{s_{NN}} = 200$ GeV

J. Adams,³ C. Adler,¹² M. M. Aggarwal,²⁵ Z. Ahammed,³⁸ J. Amonett,¹⁷ B. D. Anderson,¹⁷ M. Anderson,⁵ D. Arkhipkin,¹¹ G. S. Averichev,¹⁰ S. K. Badyal,¹⁶ J. Balewski,¹³ O. Barannikova,^{28,10} L. S. Barnby,¹⁷ J. Baudot,¹⁵ S. Bekele,²⁴ V.V. Belaga,¹⁰ R. Bellwied,⁴¹ J. Berger,¹² B. I. Bezverkhny,⁴³ S. Bhardwaj,²⁹ P. Bhaskar,³⁸ A. K. Bhati,²⁵ H. Bichsel,⁴⁰ A. Billmeier,⁴¹ L. C. Bland,² C. O. Blyth,³ B. E. Bonner,³⁰ M. Botje,²³ A. Boucham,³⁴ A. Brandin,²¹ A. Bravar,² R.V. Cadman,¹ X. Z. Cai,³³ H. Caines,⁴³ M. Calderón de la Barca Sánchez,² J. Carroll,¹⁸ J. Castillo,¹⁸ M. Castro,⁴¹ D. Cebra,⁵ P. Chaloupka,⁹ S. Chattopadhyay,³⁸ H. F. Chen,³² Y. Chen,⁶ S. P. Chernenko,¹⁰ M. Cherney,⁸ A. Chikanian,⁴³ B. Choi,³⁶ W. Christie,² J. P. Coffin,¹⁵ T. M. Cormier,⁴¹ J. G. Cramer,⁴⁰ H. J. Crawford,⁴ D. Das,³⁸ S. Das,³⁸ A. A. Derevschikov,²⁷ L. Didenko,² T. Dietel,¹² X. Dong,^{32,18} J. E. Draper,⁵ F. Du,⁴³ A. K. Dubey,¹⁴ V. B. Dunin,¹⁰ J. C. Dunlop,² M. R. Dutta Majumdar,³⁸ V. Eckardt,¹⁹ L. G. Efimov,¹⁰ V. Emelianov,²¹ J. Engelage,⁴ G. Eppley,³⁰ B. Erazmus,³⁴ M. Estienne,³⁴ P. Fachini,² V. Faine,² J. Faivre,¹⁵ R. Fatemi,¹³ K. Filimonov,¹⁸ P. Filip,⁹ E. Finch,⁴³ Y. Fisyak,² D. Flierl,¹² K. J. Foley,² J. Fu,⁴² C. A. Gagliardi,³⁵ M. S. Ganti,³⁸ T. D. Gutierrez,⁵ N. Gagunashvili,¹⁰ J. Gans,⁴³ L. Gaudichet,³⁴ M. Germain,¹⁵ F. Geurts,³⁰ V. Ghazikhanian,⁶ P. Ghosh,³⁸ J. E. Gonzalez,⁶ O. Grachov,⁴¹ V. Grigoriev,²¹ S. Gronstal,⁸ D. Grosnick,³⁷ M. Guedon,¹⁵ S. M. Guertin,⁶ A. Gupta,¹⁶ E. Gushin,²¹ T. J. Hallman,² D. Hardtke,¹⁸ J. W. Harris,⁴³ M. Heinz,⁴³ T. W. Henry,³⁵ S. Heppelmann,²⁶ T. Herston,²⁸ B. Hippolyte,⁴³ A. Hirsch,²⁸ E. Hjort,¹⁸ G. W. Hoffmann,³⁶ M. Horsley,⁴³ H. Z. Huang,⁶ S. L. Huang,³² T. J. Humanic,²⁴ G. Igo,⁶ A. Ishihara,³⁶ P. Jacobs,¹⁸ W. W. Jacobs,¹³ M. Janik,³⁹ I. Johnson,¹⁸ P. G. Jones,³ E. G. Judd,⁴ S. Kabana,⁴³ M. Kaneta,¹⁸ M. Kaplan,⁷ D. Keane,¹⁷ J. Kiryluk,⁶ A. Kisiel,³⁹ J. Klay,¹⁸ S. R. Klein,¹⁸ A. Klyachko,¹³ D. D. Koetke,³⁷ T. Kollegger,¹² A. S. Konstantinov,²⁷ M. Kopytine,¹⁷ L. Kotchenda,²¹ A. D. Kovalenko,¹⁰ M. Kramer,²² P. Kravtsov,²¹ K. Krueger,¹ C. Kuhn,¹⁵ A. I. Kulikov,¹⁰ A. Kumar,²⁵ G. J. Kunde,⁴³ C. L. Kunz,⁷ R. Kh. Kutuev,¹¹ A. A. Kuznetsov,¹⁰ M. A. C. Lamont,³ J. M. Landgraf,² S. Lange,¹² C. P. Lansdell,³⁶ B. Lasiuk,⁴³ F. Laue,² J. Lauret,² A. Lebedev,² R. Lednický,¹⁰ V. M. Leontiev,²⁷ M. J. LeVine,² C. Li,³² Q. Li,⁴¹ S. J. Lindenbaum,²² M. A. Lisa,²⁴ F. Liu,⁴² L. Liu,⁴² Z. Liu,⁴² Q. J. Liu,⁴⁰ T. Ljubicic,² W. J. Llope,³⁰ H. Long,⁶ R. S. Longacre,² M. Lopez-Noriega,²⁴ W. A. Love,² T. Ludlam,² D. Lynn,² J. Ma,⁶ Y. G. Ma,³³ D. Magestro,²⁴ S. Mahajan,¹⁶ L. K. Mangotra,¹⁶ D. P. Mahapatra,¹⁴ R. Majka,⁴³ R. Manweiler,³⁷ S. Margetis,¹⁷ C. Markert,⁴³ L. Martin,³⁴ J. Marx,¹⁸ H. S. Matis,¹⁸ Yu. A. Matulenko,²⁷ T. S. McShane,⁸ F. Meissner,¹⁸ Yu. Melnick,²⁷ A. Meschanin,²⁷ M. Messer,² M. L. Miller,⁴³ Z. Milosevich,⁷ N. G. Minaev,²⁷ C. Mironov,¹⁷ D. Mishra,¹⁴ J. Mitchell,³⁰ B. Mohanty,³⁸ L. Molnar,²⁸ C. F. Moore,³⁶ M. J. Mora-Corral,¹⁹ V. Morozov,¹⁸ M. M. de Moura,⁴¹ M. G. Munhoz,³¹ B. K. Nandi,³⁸ S. K. Nayak,¹⁶ T. K. Nayak,³⁸ J. M. Nelson,³ P. Nevski,² V. A. Nikitin,¹¹ L. V. Nogach,²⁷ B. Norman,¹⁷ S. B. Nurushev,²⁷ G. Odyniec,¹⁸ A. Ogawa,² V. Okorokov,²¹ M. Oldenburg,¹⁸ D. Olson,¹⁸ G. Paic,²⁴ S. U. Pandey,⁴¹ S. K. Pal,³⁸ Y. Panebratsev,¹⁰ S. Y. Panitkin,² A. I. Pavlinov,⁴¹ T. Pawlak,³⁹ V. Perevoztchikov,² W. Peryt,³⁹ V. A. Petrov,¹¹ S. C. Phatak,¹⁴ R. Picha,⁵ M. Planinic,⁴⁴ J. Pluta,³⁹ N. Porile,²⁸ J. Porter,² A. M. Poskanzer,¹⁸ M. Potekhin,² E. Potrebenikova,¹⁰ B. V. K. S. Potukuchi,¹⁶ D. Prindle,⁴⁰ C. Pruneau,⁴¹ J. Putschke,¹⁹ G. Rai,¹⁸ G. Rakness,¹³ R. Raniwala,²⁹ S. Raniwala,²⁹ O. Ravel,³⁴ R. L. Ray,³⁶ S. V. Razin,^{10,13} D. Reichhold,²⁸ J. G. Reid,⁴⁰ G. Renault,³⁴ F. Retiere,¹⁸ A. Ridiger,²¹ H. G. Ritter,¹⁸ J. B. Roberts,³⁰ O. V. Rogachevski,¹⁰ J. L. Romero,⁵ A. Rose,⁴¹ C. Roy,³⁴ L. J. Ruan,^{32,2} R. Sahoo,¹⁴ I. Sakrejda,¹⁸ S. Salur,⁴³ J. Sandweiss,⁴³ I. Savin,¹¹ J. Schambach,³⁶ R. P. Scharenberg,²⁸ N. Schmitz,¹⁹ L. S. Schroeder,¹⁸ K. Schweda,¹⁸ J. Seger,⁸ D. Seliverstov,²¹ P. Seyboth,¹⁹ E. Shahaliev,¹⁰ M. Shao,³² M. Sharma,²⁵ K. E. Shestermanov,²⁷ S. S. Shimanskii,¹⁰ R. N. Singaraju,³⁸ F. Simon,¹⁹ G. Skoro,¹⁰ N. Smirnov,⁴³ R. Snellings,²³ G. Sood,²⁵ P. Sorensen,⁶ J. Sowinski,¹³ H. M. Spinka,¹ B. Srivastava,²⁸ S. Stanislaus,³⁷ R. Stock,¹² A. Stolpovsky,⁴¹ M. Strikhanov,²¹ B. Stringfellow,²⁸ C. Struck,¹² A. A. P. Suaide,⁴¹ E. Sugarbaker,²⁴ C. Suire,² M. Šumbera,⁹ B. Surrow,² T. J. M. Symons,¹⁸ A. Szanto de Toledo,³¹ P. Szarwas,³⁹ A. Tai,⁶ J. Takahashi,³¹ A. H. Tang,^{2,23} D. Thein,⁶ J. H. Thomas,¹⁸ V. Tikhomirov,²¹ M. Tokarev,¹⁰ M. B. Tonjes,²⁰ T. A. Trainor,⁴⁰ S. Trentalange,⁶ R. E. Tribble,³⁵ M. D. Trivedi,³⁸ V. Trofimov,²¹ O. Tsai,⁶ T. Ullrich,² D. G. Underwood,¹ G. Van Buren,² A. M. VanderMolen,²⁰ A. N. Vasiliev,²⁷ M. Vasiliev,³⁵ S. E. Vigdor,¹³ Y. P. Viyogi,³⁸ S. A. Voloshin,⁴¹ W. Wagoner,⁸ F. Wang,²⁸ G. Wang,¹⁷ X. L. Wang,³² Z. M. Wang,³² H. Ward,³⁶ J. W. Watson,¹⁷ R. Wells,²⁴ G. D. Westfall,²⁰ C. Whitten, Jr.,⁶ H. Wieman,¹⁸ R. Willson,²⁴ S. W. Wissink,¹³ R. Witt,⁴³ J. Wood,⁶ J. Wu,³² N. Xu,¹⁸ Z. Xu,² Z. Z. Xu,³² A. E. Yakutin,²⁷ E. Yamamoto,¹⁸ J. Yang,⁶ P. Yepes,³⁰ V. I. Yurevich,¹⁰ Y. V. Zanevski,¹⁰ I. Zborovský,⁹ H. Zhang,^{43,2} H. Y. Zhang,¹⁷ W. M. Zhang,¹⁷ Z. P. Zhang,³² P. A. Żołnierczuk,¹³ R. Zoukarneev,¹¹ J. Zoukarneeva,¹¹ and A. N. Zubarev¹⁰

(STAR Collaboration)*

- ¹Argonne National Laboratory, Argonne, Illinois 60439, USA
²Brookhaven National Laboratory, Upton, New York 11973, USA
³University of Birmingham, Birmingham, United Kingdom
⁴University of California, Berkeley, California 94720, USA
⁵University of California, Davis, California 95616, USA
⁶University of California, Los Angeles, California 90095, USA
⁷Carnegie Mellon University, Pittsburgh, Pennsylvania 15213, USA
⁸Creighton University, Omaha, Nebraska 68178, USA
⁹Nuclear Physics Institute AS CR, Řež/Prague, Czech Republic
¹⁰Laboratory for High Energy (JINR), Dubna, Russia
¹¹Particle Physics Laboratory (JINR), Dubna, Russia
¹²University of Frankfurt, Frankfurt, Germany
¹³Indiana University, Bloomington, Indiana 47408, USA
¹⁴Institute of Physics, Bhubaneswar 751005, India
¹⁵Institut de Recherches Subatomiques, Strasbourg, France
¹⁶University of Jammu, Jammu 180001, India
¹⁷Kent State University, Kent, Ohio 44242, USA
¹⁸Lawrence Berkeley National Laboratory, Berkeley, California 94720, USA
¹⁹Max-Planck-Institut für Physik, Munich, Germany
²⁰Michigan State University, East Lansing, Michigan 48824, USA
²¹Moscow Engineering Physics Institute, Moscow, Russia
²²City College of New York, New York City, New York 10031, USA
²³NIKHEF, Amsterdam, The Netherlands
²⁴The Ohio State University, Columbus, Ohio 43210, USA
²⁵Panjab University, Chandigarh 160014, India
²⁶Pennsylvania State University, University Park, Pennsylvania 16802, USA
²⁷Institute of High Energy Physics, Protvino, Russia
²⁸Purdue University, West Lafayette, Indiana 47907, USA
²⁹University of Rajasthan, Jaipur 302004, India
³⁰Rice University, Houston, Texas 77251, USA
³¹Universidade de Sao Paulo, Sao Paulo, Brazil
³²University of Science & Technology of China, Anhui 230027, China
³³Shanghai Institute of Nuclear Research, Shanghai 201800, People's Republic of China
³⁴SUBATECH, Nantes, France
³⁵Texas A&M, College Station, Texas 77843, USA
³⁶University of Texas, Austin, Texas 78712, USA
³⁷Valparaiso University, Valparaiso, Indiana 46383, USA
³⁸Variable Energy Cyclotron Centre, Kolkata 700064, India
³⁹Warsaw University of Technology, Warsaw, Poland
⁴⁰University of Washington, Seattle, Washington 98195, USA
⁴¹Wayne State University, Detroit, Michigan 48201, USA
⁴²Institute of Particle Physics, CCNU (HZNU), Wuhan, 430079 China
⁴³Yale University, New Haven, Connecticut 06520, USA
⁴⁴University of Zagreb, Zagreb, HR-10002, Croatia
(Received 2 October 2003; published 18 March 2004)

Transverse mass and rapidity distributions for charged pions, charged kaons, protons, and antiprotons are reported for $\sqrt{s_{NN}} = 200$ GeV pp and Au + Au collisions at Relativistic Heavy Ion Collider (RHIC). Chemical and kinetic equilibrium model fits to our data reveal strong radial flow and long duration from chemical to kinetic freeze-out in central Au + Au collisions. The chemical freeze-out temperature appears to be independent of initial conditions at RHIC energies.

DOI: 10.1103/PhysRevLett.92.112301

PACS numbers: 25.75.Dw

Quantum chromodynamics predicts a phase transition from hadronic matter to quark-gluon plasma (QGP) at critical temperature $T_c \approx 170$ MeV, at extreme conditions of high energy density, possibly achieved in relativistic heavy-ion collisions [1]. Signals of QGP may remain in the bulk properties of the collision, and simultaneous observations of multiple QGP signals in the final

state serve as strong evidence of QGP formation. These bulk properties include strangeness and baryon production rates, collective transverse radial flow, and system temperature. These can be studied via particle spectra.

In this Letter we report results on charged pion (π^\pm), charged kaon (K^\pm), proton (p), and antiproton (\bar{p}) production from pp and Au + Au collisions at Relativistic

Heavy Ion Collider (RHIC) by the STAR experiment at the nucleon-nucleon center-of-mass energy of $\sqrt{s_{NN}} = 200$ GeV. In some models it is argued that particle multiplicity density per transverse area of interaction measures the initial gluon density [2], particle ratios measure the chemical freeze-out conditions [3], and transverse momentum spectra measure the kinetic freeze-out conditions [4]. We study these properties at midrapidity as a function of centrality. The rapidity dependences of particle production and spectra shape are also investigated.

Charged particles are detected in the STAR time projection chamber (TPC) [5]. The TPC is surrounded by a solenoidal magnet providing a uniform magnetic field of 0.5 T along the beam line. Zero degree calorimeters and beam-beam counters [6] provide a minimum bias trigger for Au + Au and pp collisions, respectively. Events with a primary vertex within ± 25 cm of the geometric center of the TPC along the beam axis are accepted. For this analysis, about 2.0×10^6 Au + Au and about 2.5×10^6 pp minimum bias accepted events are used. Only primary tracks—tracks pointing to the primary vertex within 3 cm—are selected. The Au + Au events are divided into nine centrality classes based on measured charged particle multiplicity within pseudorapidity $|\eta| < 0.5$. These classes consist, from central to peripheral, of (0–5)%, (5–10)%, (10–20)%, (20–30)%, (30–40)%, (40–50)%, (50–60)%, (60–70)%, and (70–80)% of the geometrical cross section.

Particle identification is accomplished by measuring the ionization energy loss dE/dx . The mean $\langle dE/dx \rangle$ is determined from 70% of the samples with the lowest dE/dx along a track. To ensure good momentum and $\langle dE/dx \rangle$ resolution, tracks are required to have at least 25 out of the maximum 45 hits in the TPC. The $\langle dE/dx \rangle$ resolution varies between 6% and 10% from pp to central Au + Au events. The reconstructed momenta are corrected most likely for energy loss in the detector. The correction is negligible for π^\pm , under 2% for K^\pm and under 5% for p and \bar{p} in the covered momentum ranges. The momentum resolution was estimated to be about 2% at $p_\perp = 0.5$ GeV/ c . Uncorrected particle yields are extracted from $\langle dE/dx \rangle$ distributions for each p_\perp , rapidity and centrality bin [7–10].

Corrections are applied to account for tracking inefficiency, detector acceptance, hadronic interactions, and particle decays. The total reconstruction efficiencies are obtained from embedding Monte Carlo (MC) tracks into real events at the raw data level and subsequently reconstructing these events. The propagation of single tracks is calculated using GEANT, a detailed description of the STAR geometry, and a realistic simulation of the TPC response [7–10]. The efficiencies for π^\pm are (50–70)% and (80–90)% in the covered p_\perp for the (0–5)% and (70–80)% events, respectively. The corresponding efficiencies for K^\pm are (20–50)% and (40–70)% and for p and \bar{p} (70–75)% and (75–80)%. Background protons knocked out

from the detector material are subtracted. This background is (50–60)% at $p_\perp = 0.4$ GeV/ c and becomes less than 5% at 1.0 GeV/ c [8].

Corrections for the pp data are similar to those for the (70–80)% Au + Au events. Additional corrections are applied for primary vertex reconstruction inefficiency and fake events (events with misreconstructed vertex due to the pileup background). These corrections are obtained by embedding HIJING [11] events into events that had been triggered on empty bunches, and reconstructing the combined events. The vertex reconstruction inefficiency strongly decreases with increasing event multiplicity resulting in approximately 14% of the events being missed, over 80% of which have fewer than three tracks in the TPC. About 12% of pp events are fake events with reconstructed multiplicity about half of that of real events due to time distortion in the pileup background, resulting in an overall correction of (6–8)% in the covered p_\perp range.

The pion spectra are further corrected for weak decay products, muon contamination, and background pions produced in the detector material. The resulting correction is approximately 12%. Because weak decay (anti)protons carry most of the parent momentum, their tracks behave as those originating from the primary vertex, resulting in the same reconstruction efficiency for weak decay and primary (anti)protons over the measured p_\perp range. The inclusive (anti)protons closely reflect total (anti)baryon production [7,8]. Therefore, we present inclusive proton and antiproton distributions that are not corrected for weak decays. Based on the measured Λ distribution [12], we estimate that about 40% of the measured protons are from weak decays, and the measured inclusive $\langle p_\perp \rangle$ are similar to those of primary protons.

The point to point systematic uncertainties on the spectra are estimated by varying event and track selection and analysis cuts and by assessing sample purity from the dE/dx measurement. The estimated uncertainties are less than 4% for π^\pm , p , and \bar{p} . Those for K^\pm are less than 12% for p_\perp bins with significant overlap in dE/dx with e^\pm or π^\pm , and less than 4% for other bins. An additional systematic error on the proton spectra due to background subtraction is estimated to be 5% at low p_\perp and negligible at high p_\perp [8]. A correlated systematic uncertainty of 5% is estimated for all spectra and is dominated by uncertainties in the MC determination of reconstruction efficiencies.

Figure 1 shows transverse mass ($m_\perp = \sqrt{p_\perp^2 + m^2}$) spectra for π^\pm , K^\pm , p , and \bar{p} for pp and all centrality bins of Au + Au data within $|y| < 0.1$. For clarity, proton spectra are scaled by 0.8. While the π^\pm spectra shapes are similar for pp and Au + Au, K^\pm , p , and \bar{p} spectra show a progressive flattening from pp to central Au + Au events. Similar trends were also observed for Au + Au collisions

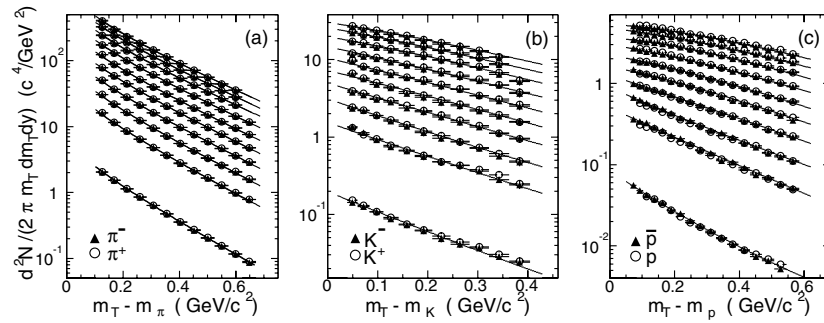


FIG. 1. Invariant yield as functions of transverse mass for π^\pm , K^\pm , and inclusive p and \bar{p} at midrapidity ($|y| < 0.1$) for pp (bottom) and Au + Au events from (70–80)% (second from bottom) to the (0–5)% centrality bin (top). The curves shown are explained in the text.

by PHENIX [13]. Our pp results are consistent with previous measurements at similar multiplicities [14].

The blast-wave model—a hydrodynamically motivated model with a kinetic freeze-out temperature T_{kin} and a transverse flow velocity field β [4]—can simultaneously fit the K^\pm , p , and \bar{p} spectra and the high- p_\perp part ($p_\perp > 0.50$ GeV/ c) of the π^\pm spectra. We used a velocity profile of $\beta = \beta_s(r/R)^n$, where $r \leq R$ (the term r/R accounts for the change in the velocity as a function of radial distance), β_s is the surface velocity, and n is treated as a free parameter. The value of n ranges from 1.50 ± 0.29 in peripheral to 0.82 ± 0.02 in central events. The fit results are superimposed in Figs. 1(b) and 1(c). The obtained fit parameters for the (0–5)% Au + Au events are $T_{\text{kin}} = 89 \pm 10$ MeV and $\langle\beta\rangle = 0.59 \pm 0.05$, $\beta_s = 0.84 \pm 0.07$, and are similar to the 130 GeV results reported in [9,14]. The systematic uncertainties in the fit parameters are estimated by excluding the kaon or the (anti)proton spectra from the fit.

Recent attempts to fit the measured RHIC spectra with a single (chemical and kinetic) freeze-out temperature claim this is possible if all the resonance and weak decay feed downs are taken into account [16]. Our MC study of that scenario shows significantly higher χ^2/NDF compared to our blast-wave fits.

The low- p_\perp part of the pion spectrum deviates from the blast-wave model description, possibly due to large contributions from resonances at low p_\perp . We fit the pion spectra to a Bose-Einstein distribution [$\propto 1/(\exp(\frac{m_T}{T}) - 1)$], the results of which are superimposed in Fig. 1(a). The yields outside the measured p_\perp region are extrapolated using the blast-wave model for K^\pm , p , and \bar{p} and the Bose-Einstein distribution for π^\pm . The extrapolation is approximately 30% for pions, and varies with centrality from about 35% to 55% for kaons and (anti)protons. The uncertainties on these extrapolations are estimated by comparing to results using other functional forms. The estimated extrapolation uncertainties in the $\langle p_\perp \rangle$ and total yield are 5% for π^\pm and 5% to 10% for K^\pm , p , and \bar{p} (varying from pp to central Au + Au collisions). For the (0–5)% Au + Au collisions, the integrated yields are

$dN/dy = 322 \pm 32$ for π^+ , 327 ± 33 for π^- , 51.3 ± 7.7 for K^+ , 49.5 ± 7.4 for K^- , 34.7 ± 6.2 for p , and 26.7 ± 4.0 for \bar{p} . The obtained \bar{p}/p ratio for the 0%–5% Au + Au collisions is 0.77 ± 0.05 , indicating a nearly net-baryon free midrapidity region at this RHIC energy.

We extract the fiducial dN/dy by summing up the yields within the p_\perp range of 0.20–0.70 GeV/ c for π^- , 0.25–0.60 GeV/ c for K^- , and 0.50–1.05 GeV/ c for \bar{p} . Figure 2 depicts the rapidity dependence of the fiducial dN/dy and extrapolated $\langle p_\perp \rangle$ for the (0–5)% and (70–80)% Au + Au events. We do not observe changes in either shape or yield for any particle species within $|y| < 0.5$. The pp data and all other centrality bins of the Au + Au data exhibit the same behavior. Such an absence of rapidity dependence of particle spectra was also observed for π^\pm , p , and \bar{p} at $\sqrt{s_{NN}} = 130$ GeV Au + Au collisions [8,9]. This uniformity indicates the development of a boost-invariant region within the measured kinematic ranges.

The centrality dependence of the extracted $\langle p_\perp \rangle$ within $|y| < 0.1$ is shown in Fig. 3(a). A smooth changeover from pp to peripheral Au + Au collisions is observed for all particle species. The $\langle p_\perp \rangle$ increases from pp and peripheral Au + Au to central Au + Au collisions, especially for p , \bar{p} , and K^\pm . This behavior is consistent with an increase of radial flow with collision centrality.

The K^-/π^- and \bar{p}/π^- ratios of the integrated dN/dy yields within $|y| < 0.1$ are depicted in Fig. 3(b). We observe little centrality dependence of the K^-/π^- or \bar{p}/π^-

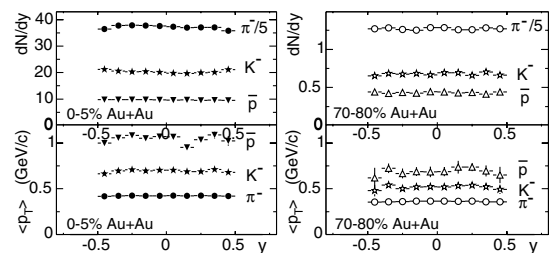


FIG. 2. Rapidity distributions of the fiducial yields and integrated $\langle p_\perp \rangle$.

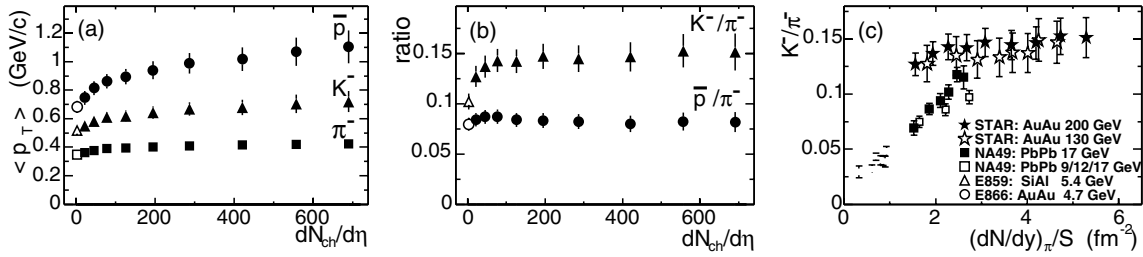


FIG. 3. (a) $\langle p_{\perp} \rangle$ and (b) K^{-}/π^{-} and \bar{p}/π^{-} as a function of $dN_{ch}/d\eta$. (c) Midrapidity K^{-}/π as a function of $\sqrt{(dN/dy)_{\pi}}/S$. Systematic errors are shown for STAR data, and statistical errors for other data.

ratio from midcentral to central Au + Au collisions, indicating a similar freeze-out condition in these collisions. Similar centrality behavior has been observed for other particle ratios measured at $\sqrt{s_{NN}} = 200$ and 130 GeV [8,10].

The observed centrality independence of K^{-}/π^{-} is in contrast to low energy data at Super Proton Synchrotron (SPS) [17] and Alternating Gradient Synchrotron (AGS) [18], where a continuous increase in K^{-}/π was observed, roughly doubling from peripheral to central collisions. To put our results into perspective with low energy data, we plot in Fig. 3(c) the K^{-}/π ratio as a function of $\frac{(dN/dy)_{\pi}}{S}$, in an attempt to reflect effects of both the collision energy and centrality. Here S is an estimate of the transverse overlap area: $S = \pi[1.12(N_{part}/2)^{1/3}]^2$, where number of participants N_{part} is experimentally measured for the AGS and SPS data and calculated via the MC Glauber model for RHIC data [9]. The $\frac{(dN/dy)_{\pi}}{S}$ may be related to the initial conditions of the collision [2,19], such as energy density. In high energy collisions the initial gluon density is saturated up to a momentum scale that is proportional to $\sqrt{(dN/dy)_{\pi}/S}$ [2]. Using data over a wide range of collision energy measured in various colliding systems, Fig. 3(c) shows a distinct change in the ratio behavior. Low energy measurements (each representing approximately the top 60% of the geometrical cross section) appear to follow a trend that saturates at RHIC energies. One interpretation of this is that strangeness production at low energies depends on how the collision was initially prepared, but not at RHIC energies. On the other hand, the K^{+}/π and \bar{p}/π ratios display a different behavior with $\frac{(dN/dy)_{\pi}}{S}$. However, we note that the net-baryon density, significant at low energies, greatly affects K^{+} and \bar{p} abundances through associated production of K^{+} with baryons [10] and baryon-antibaryon annihilation [20], respectively.

In the framework of a chemical-equilibrium model [3,21], integrated yield ratios can be described by a set of parameters: the chemical freeze-out temperature (T_{ch}), the baryon and strangeness chemical potentials (μ_B , μ_s), and the strangeness suppression factor (γ_s). We fit our measured ratios with such a model to extract these parameters. The value obtained for the chemical potential, $\mu_B \approx 22 \pm 4$ MeV, is independent of centrality within

errors, and μ_s is consistent with 0. The obtained γ_s increases from 0.56 ± 0.04 in pp to 0.86 ± 0.11 in central Au + Au collisions reflecting the measured K/π ratios. The obtained T_{ch} is summarized in Fig. 4 as a function of charged hadron multiplicity, together with T_{kin} and $\langle \beta \rangle$ extracted from the blast-wave model fit to our data. As seen in Fig. 4, $\sqrt{(dN/dy)_{\pi}}/S$ increases with centrality, T_{ch} is independent of it, T_{kin} decreases, and $\langle \beta \rangle$ increases with centrality. This suggests that Au + Au collisions of different initial conditions always evolve to the same chemical freeze-out condition, and then cool down further to a kinetic freeze-out dependent on centrality. The expansion of the system gives rise to collective flow.

During expansion from chemical to kinetic freeze-out, entropy density drops approximately as T^3 [22], implying that the system size at kinetic freeze-out is at least a factor of $\frac{T_{ch}}{T_{kin}}$ of the size at chemical freeze-out. This suggests a time span from chemical to kinetic freeze-out in central collisions is at least of the order of $\Delta t \approx (\frac{T_{ch}}{T_{kin}} - 1)R/\beta_s \approx 6$ fm/c. Here we have taken $R = 6$ fm, the Au nuclei radius, as an estimate of the system size at chemical freeze-out.

In summary, we have reported transverse mass and rapidity distributions of π^{\pm} , K^{\pm} , p , and \bar{p} for pp and Au + Au collisions at $\sqrt{s_{NN}} = 200$ GeV at RHIC. A boost-invariant region of at least $\Delta y \approx 1$ is developed at midrapidity for particles within our measured p_{\perp} range.

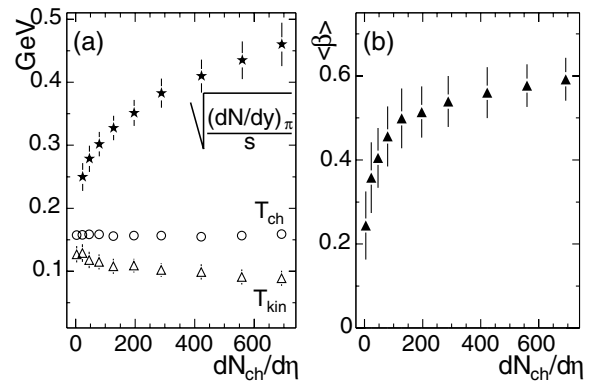


FIG. 4. (a) $\sqrt{(dN/dy)_{\pi}}/S$ (stars), T_{ch} (circles), and T_{kin} (triangles), and (b) $\langle \beta \rangle$ as a function of $dN_{ch}/d\eta$. Errors are systematic.

The spectra are well described by the blast-wave model, yielding a decreasing T_{kin} and increasing $\langle\beta\rangle$ with centrality, reaching the values of $T_{\text{kin}} = 89 \pm 10$ MeV and $\langle\beta\rangle = 0.59 \pm 0.05$ in the 5% most central collisions. Particle ratios vary smoothly from pp to peripheral Au + Au and remain relatively constant from midcentral to central Au + Au collisions. The K^-/π ratio from various collisions over a wide range of energy reveals a distinct behavior in $\frac{(dN/dy)_\pi}{S}$. A chemical-equilibrium model fit to the ratios yields a T_{ch} insensitive to centrality with a value of 157 ± 6 MeV for the 5% most central collisions. The drop in temperature from T_{ch} to T_{kin} and the development of strong radial flow suggest a significant expansion and long duration from chemical to kinetic freeze-out in central collisions. From these results the following picture seems to emerge at RHIC: collision systems with varying initial conditions always evolve towards the same chemical freeze-out condition followed by cooling and expansion of increasing magnitude with centrality.

We thank the RHIC Operations Group and RCF at BNL, and the NERSC Center at LBNL for their support. This work was supported in part by the HENP Divisions of the Office of Science of the U.S. DOE; the U.S. NSF; the BMBF of Germany; IN2P3, RA, RPL, and EMN of France; EPSRC of the United Kingdom; FAPESP of Brazil; the Russian Ministry of Science and Technology; the Ministry of Education and the NNSFC of China; Grant Agency of the Czech Republic, DAE, DST, and CSIR of the Government of India; the Swiss NSF.

*Electronic address: www.star.bnl.gov

- [1] F. Karsch, Nucl. Phys. **A698**, 199c (2002).
 [2] D. Kharzeev and E. Levin, Phys. Lett. B **523**, 79 (2001).

- [3] P. Braun-Munzinger, I. Heppe, and J. Stachel, Phys. Lett. B **465**, 15 (1999).
 [4] E. Schnedermann, J. Sollfrank, and U. Heinz, Phys. Rev. C **48**, 2462 (1993).
 [5] K. H. Ackermann *et al.*, Nucl. Instrum. Methods Phys. Res., Sect. A **499**, 624 (2003).
 [6] J. Adams *et al.*, Phys. Rev. Lett. **91**, 172302 (2003).
 [7] C. Adler *et al.*, Phys. Rev. Lett. **87**, 262302 (2001).
 [8] J. Adams *et al.*, nucl-ex/0306029; C. Adler *et al.*, Phys. Rev. Lett. **86**, 4778 (2001); **90**, 119903 (2003).
 [9] J. Adams *et al.*, nucl-ex/0311017.
 [10] C. Adler *et al.*, nucl-ex/0206008.
 [11] X.-N. Wang and M. Gyulassy, Phys. Rev. D **44**, 3501 (1991).
 [12] C. Adler *et al.*, Phys. Rev. Lett. **89**, 092301 (2002).
 [13] S. S. Adler *et al.*, nucl-ex/0307022.
 [14] C. Albajar *et al.*, Nucl. Phys. **B335**, 261 (1990); T. Alexopoulos *et al.*, Phys. Rev. D **48**, 984 (1993).
 [15] C. Adler *et al.*, Phys. Rev. Lett. **87**, 182301 (2001).
 [16] A. Baran, W. Broniowski, and W. Florkowski, Acta Phys. Pol. B **35**, 779 (2004).
 [17] F. Siklér, Nucl. Phys. **A661**, 45c (1999); I. G. Bearden *et al.*, Phys. Lett. B **471**, 6 (1999); H. Bøggild *et al.*, Phys. Rev. C **59**, 328 (1999); S. V. Afanasiev *et al.*, Phys. Rev. C **66**, 054902 (2002).
 [18] T. Abbott *et al.*, Phys. Rev. Lett. **66**, 1567 (1991); Phys. Rev. D **45**, 3906 (1992); Phys. Rev. C **50**, 1024 (1994); L. Ahle *et al.*, Phys. Rev. C **60**, 044904 (1999); **58**, 3523 (1998); **57**, 466 (1998); L. Ahle *et al.*, Phys. Lett. B **476**, 1 (2000); **490**, 53 (2000).
 [19] J. D. Bjorken, Phys. Rev. D **27**, 140 (1983).
 [20] M. Bleicher *et al.*, Phys. Lett. B **485**, 133 (2000); F. Wang, J. Phys. G **27**, 283 (2001).
 [21] N. Xu and M. Kaneta, Nucl. Phys. **A698**, 306c (2002).
 [22] C. Y. Wong, *Introduction to High Energy Heavy-Ion Collisions* (World Scientific, Singapore, 1994).